CHEMISTRY OF MATERIALS
Article

Chem. Mater. **2010,** *22,* 2681–2684 2681
DOI:10.1021/cm100418w

Synthesis of Vertically Aligned Hollow Platinum Nanotubes with Single Crystalline Nanoflakes

Lichun Liu,[†] Sang-Hoon Yoo,[†] and Sungho Park*[,†,‡,§]

[†]*Department of Chemistry, Sungkyunkwan University, Suwon 440-746, South Korea,* [‡]*Department of Energy Science, Sungkyunkwan University, Suwon 440-746, South Korea, and* [§]*SKKU Advanced Institute of Nanotechnology, Sungkyunkwan University, Suwon 440-746, South Korea*

Received February 9, 2010

This paper reports on a methodology for synthesizing vertical arrays of hollow platinum nanotubes with [111] single-crystalline nanoflakes. Initially, single-component nickel nanorods were fabricated with the aid of AAO templates and electrochemical deposition. When the resulting nickel nanorods were immersed in a Pt-ion-containing aqueous solution, the nickel metal dissolved into Ni^{2+} ions through spontaneous galvanic replacement with Pt ions. However, the direct replacement between nickel nanorods and Pt ions led to an irregular architecture in the resulting deposition of platinum. Instead, a pitting corrosion pretreatment of the nickel nanorods produced nucleation sites for replacement with the Pt ions. This step was critical for accelerating the interfacial replacement reaction rate and the formation of the regular platinum nanotubes with ultrathin superficial nanoflakes. We found that the Kirkendall effect was operative in the formation of platinum nanotubes.

Introduction

Hollow nanomaterials covering porous nanomaterials are of critical importance in advanced applications in modern science and technology, such as catalysis, photonics, and drug delivery,[1] principally because of their high surface area, low density, and usable nanoscale inner space. Since platinum-based nanomaterials play key roles in many catalysis processes, because of their distinct chemical and physical properties,[2] a wide variety of research has focused on the synthesis of novel hollow platinum nanostructures to maximize the use of platinum, compared to its solid counterparts.

A large number of alloyed platinum hollow nanostructures with definitely higher surface-area:mass ratios have readily been fabricated by controlling the concentration of reduction agent, using direct thermolytic reduction, an in situ sacrificial template, and colloidal templating.[3] For example, using cobalt nanoparticles as sacrificial templates, Liang and co-workers have synthesized colloidal platinum hollow nanospheres, exhibiting enhanced electrocatalytic activity for the oxidation of methanol.[4] Given the advantages of interconnected nanopores and nanochannels in porous gold substrates via the dealloying of Au−Ag alloys,[5] a large surface area of subnanometer-thick platinum coating can be generated using a underpotential deposition (UPD) process.[6] More-diverse recipes for synthesizing porous platinum nanostructures have also been reported.[7] Porous-like platinum film with all-over nanorod arrays has a highly accessible effective surface area, because of the generation of a large side surface of vertically aligned length-tunable nanorods. However, the surface-area:mass ratio of platinum nanorods is confined by their solid interiors and smooth surfaces. An effective and straightforward method to enhance the surface area: mass ratio is to hollow the interior and roughen the surfaces of these nanorod materials. Herein, we demonstrate a facile approach for fabricating novel vertical hollow platinum nanotube arrays with epitaxial single-crystalline superficial thin nanoflakes.

Experimental Section

AAO membrane templates (diameter ≈ 25 mm, pore size ≈ 200 nm, thickness ≈ 60 μm) were purchased from Whatman

*Author to whom correspondence should be addressed. Fax: 82-31-290-7075. E-mail: spark72@skku.edu.

(1) (a) Lim, B.; Jiang, M. J.; Camargo, P. H. C.; Cho, E. C.; Tao, J.; Lu, X. M.; Zhu, Y. M.; Xia, Y. A. *Science* **2009**, *324*(5932), 1302–1305. (b) Cregan, R. F.; Mangan, B. J.; Knight, J. C.; Birks, T. A.; Russell, P. S. J.; Roberts, P. J.; Allan, D. C. *Science* **1999**, *285*(5433), 1537–1539. (c) Im, S. H.; Jeong, U.; Xia, Y. *Nat. Mater.* **2005**, *4*(9), 671–675.
(2) (a) Liu, P.; Ge, X.; Wang, R.; Ma, H.; Ding, Y. *Langmuir* **2009**, *25* (1), 561–567. (b) Chen, J.; Herricks, T.; Geissler, M.; Xia, Y. *J. Am. Chem. Soc.* **2004**, *126*(35), 10854–10855.
(3) (a) Liang, H. P.; Guo, Y. G.; Zhang, H. M.; Hu, J. S.; Wan, L. J.; Bai, C. L. *Chem. Commun.* **2004**, *13*, 1496–1497. (b) Chen, G.; Xia, D.; Nie, Z.; Wang, Z.; Wang, L.; Zhang, L.; Zhang, J. *Chem. Mater.* **2007**, *19*(7), 1840–1844. (c) Vasquez, Y.; Sra, A. K.; Schaak, R. E. *J. Am. Chem. Soc.* **2005**, *127*(36), 12504–12505. (d) Lu, L.; Sun, G.; Xi, S.; Wang, H.; Zhang, H.; Wang, T.; Zhou, X. *Langmuir* **2003**, *19*(7), 3074–3077.
(4) Liang, H.-P.; Zhang, H.-M.; Hu, J.-S.; Guo, Y.-G.; Wan, L.-J.; Bai, C.-L. *Angew. Chem., Int. Ed.* **2004**, *43*(12), 1540–1543.
(5) (a) Erlebacher, J.; Aziz, M. J.; Karma, A.; Dimitrov, N.; Sieradzki, K. *Nature* **2001**, *410*(6827), 450–453. (b) Forty, A. J. *Nature* **1979**, *282*(5739), 597–598.
(6) (a) Yoo, S. H.; Park, S. *Adv. Mater.* **2007**, *19*(12), 1612–1615. (b) Shin, T. Y.; Yoo, S. H.; Park, S. *Chem. Mater.* **2008**, *20*(17), 5682–5686.
(7) Xie, J.; Zhang, Q.; Zhou, W.; Lee, J. Y.; Wang, D. I. C. *Langmuir* **2009**, *25*(11), 6454–6459.

Published on Web 03/02/2010

International. Gold and nickel plating solutions were obtained from Technic, Inc., and Hantech PMC, respectively. Sulfuric acid (99.999%) was obtained from Sigma−Aldrich. H_2PtCl_6 was obtained from Kojima Chemicals. Deionized (DI) water (Millipore Milli-Q, with a resistivity of $\rho > 18.2$ MΩ cm) was used in all aqueous solutions.

Autolab ATU12 equipped with a three-compartment electrochemical Teflon cell was used for electrochemical depositions and CV measurements. A platinum mesh and Ag/AgCl (3 M KCl) electrode were employed as the counterelectrode and reference electrode, respectively. A JEOL Model JSM-7401F field-emission scanning electron microscopy (FE-SEM) system was used to acquire SEM images, and a JEOL Model JEM2100F high-resolution transmission electron microscopy (HR-TEM) system was used to acquire TEM images. Nanorods and nanotubes were attached on a carbon tape for the acquisition of SEM images. Platinum nanotubes were dissociated from the gold bottom via mechanical agitation, using sonication, and they were dispersed on a copper grid for TEM observations. The solid platinum nanorod and hollow platinum nanotube arrays on a glassy carbon plate were assembled into a Teflon cell and used as a working electrode for electrochemical study.

Gold nanoparticles as a conducting layer on the mesh side of AAO was prepared, employing our previously proposed method.[8] Then, gold was deposited at −0.95 V by passing 0.5 Coulombs into a 0.5 cm^2 ring-sealed AAO template to fill interparticle voids formed in the conducting layer. Subsequently, nickel was typically deposited at −0.95 V by passing 1.5 Coulombs. (For the case of platinum nanorods, 2 Coulombs were used for deposition at −0.3 V in a solution containing 0.1 M H_3BO_3 and 20 mM H_2PtCl_6.) The resulting AAO template was totally removed by 3 M NaOH for 1 h in situ in a Teflon cell and rinsed five times by DI water. For the pitting corrosion process of nickel nanorods, 1 mL of 0.5 M H_2SO_4 was placed into a Teflon cell for 10 min and then followed by rinsing five times using DI water. Finally, 1 mL of 2.5 mM H_2PtCl_6 solution was cast into a Teflon cell and maintained for 2 h for galvanic replacement reaction at room temperature, to form vertical platinum nanotubes.

Cyclic votammetry (CV) measurements were performed at a scanning rate of 50 mV/s in a 0.1 M H_2SO_4 solution under N_2 purging. Specific electrochemical surface area (ECSA) was estimated using a hydrogen monolayer adsorption/desorption method,[9] using the following equation:

$$\mathrm{ECSA} = \frac{S_{\mathrm{ad}}}{rcm}$$

where S_{ad} denotes the integration area of a hydrogen desorption peak (expressed in units of V A), r the scan rate used in cyclic votammetry (expressed in units of V/s), c the charge density (c = 210 $\mu C/cm^2$) for hydrogen UPD region, and m the mass of working electrode material (given in grams). The adlayer of CO was formed by purging with CO gas, followed by N_2 sparging to remove CO from the electrolyte solution.

Results and Discussion

Chloroplatinic acid (H_2PtCl_6), which is the most commonly used noble platinum compound, has a relatively high redox potential ($PtCl_6^{2+}/Pt$, 0.74 V vs SHE)[3] and is liable to react with other less-active elemental metals, such as Ni (Ni^{2+}/Ni, −0.26 V vs SHE), abiding by the redox replacement reactions ($PtCl_6^{2-} + 2Ni \rightarrow Pt + 6Cl^- + 2Ni^{2+}$). The potential redox difference between H_2PtCl_6 (the platinum precursor) and nickel (the sacrificial template) results in the production of elemental platinum. We first fabricated vertical nickel nanorod arrays, exploiting a facile bottom-up approach via electrodeposition with the aid of AAO membrane templates. Next, we conducted a galvanic replacement reaction by simply casting 1 mL of 2.5 mM H_2PtCl_6 solution onto nickel nanorod arrays film in an in situ Teflon electrochemical compartment. We found that direct casting of solution containing excess H_2PtCl_6 (Pt/Ni = 0.6, on a molar basis) onto as-synthesized nickel nanorod array films can lead to the replacement reaction; however, the resulting nanorods exhibited a collapsed morphology (see Figure S1 in the Supporting Information).

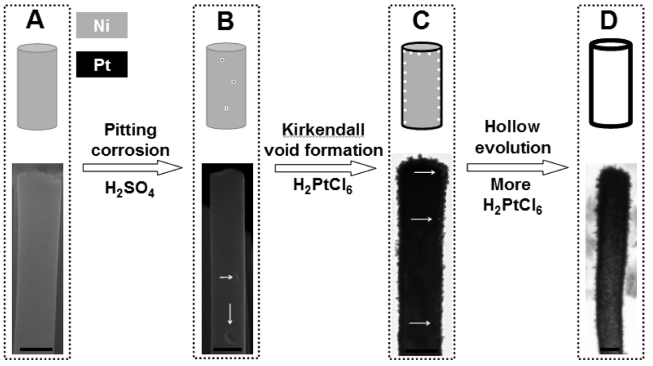

Figure 1. Schematic illustration (top panel) for synthesis process of hollow platinum nanotubes and their corresponding SEM (A and B) and TEM (C and D) images (bottom panel). White arrows indicate the pits on the surface of nanorods. Scale bars on the bottom indicate 200 nm.

On the other hand, by deploying a pretreatment of 0.5 M H_2SO_4 for 10 min before casting the H_2PtCl_6 solution onto the nickel nanorod array films, we obtained vertical platinum nanotube arrays (see Figure 1D). We found that the pretreatment of 10 min, under the given acidic conditions, leads to the best resulting platinum nanotubular structures. If the immersion time is longer than this time period, it causes a collapse of the platinum nanotubes. The mild acid pretreatment procedure induced the formation of random pit defect sites on the surfaces of the nickel nanorods (see Figure 1B). The surface morphologies of the nickel nanorods was dependent on the time of the interaction with H_2SO_4 (see Figure 2). These pit defect sites are phenomenally analogous to those of conventional pitting corrosion, which occurs in normal metals in a sporadic, localized, and stochastic fashion through a defect site. The random pits produced on the nickel nanorod surface strongly indicate the existence of crystallographic defect sites on the surfaces of the polycrystalline nickel nanorods. The disruption of interatom bonds of Ni at defect regions by H_2SO_4 increased the interfacial surface area (i.e., excess surface free energy). The $PtCl_6^{2-}$ anions, driven by concentration diffusion, approached the surface from the top to the bottom of the

(8) Yoo, S.-H.; Liu, L.; Park, S. *J. Colloid Interface Sci.* **2009**, *339*(1), 183–186.
(9) Lim, B.; Jiang, M. J.; Camargo, P. H. C.; Cho, E. C.; Tao, J.; Lu, X. M.; Zhu, Y. M.; Xia, Y. A. *Science* **2009**, *324*(5932), 1302–1305.

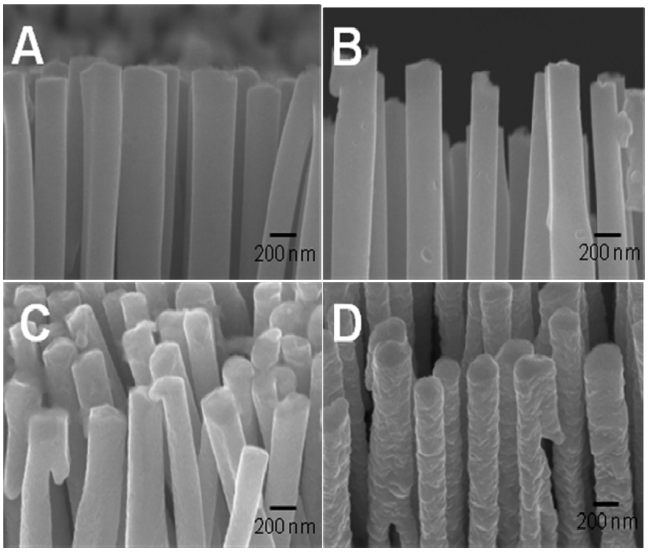

Figure 2. (A) SEM image showing the vertical nickel nanorod array before immersing into 0.5 M H_2SO_4 solution. Also shown are SEM images that reveal the morphological change on the surface of the nanorods after immersing into H_2SO_4 solution for (B) 10 min, (C) 30 min, and (D) 60 min.

nanorods and preferentially reacted with Ni on the surface defect regions, yielding Ni^{2+} and Pt atoms. In the initial stage, inward slow-moving reduced Pt atoms incapable of filling the original positions of the 2-fold stoichiometric Ni atoms, which become outward fast-moving oxidized Ni^{2+}, initiated the generation of the Kirkendall void[10] (see Figure 1C). Before these voids reached their critical coalescence size, the yielded platinum shell and nickel core were not completely separated from each other. Discrete vacancies were formed at the interface of the platinum shell and nickel core (see Figure 3). A galvanic replacement reaction continuously proceeded with the nickel core acting as the anode and the platinum shell acting as the cathode. Simultaneous surface diffusion[11] and Ostwald ripening[12] evolves the Kirkendall voids, which are the result of the Ni core separating from the Pt shell. The continuously reduced Pt atoms epitaxially dwell on the initial platinum shell until the nickel core is completely consumed, forming a fully hollow interior. Scanning electron microscopy (SEM) (Figure 4A) and transmission electron microscopy (TEM) (Figure 4B) observations corroborated that the final products were completely hollow nanotube structures when there was a sufficient amount of H_2PtCl_6 to replace all of the nickel.

Because of the vertical concentration gradient of H_2PtCl_6 solution on the nanorod array films during the replacement reaction, a higher percentage of platinum on the tops of the nanorods was reduced, compared to that on the bottoms of the nanorods. Since the electrons released from the Ni atoms can easily migrate to the top of the nanorods through the metal surface, to be consumed by high concentration of H_2PtCl_6, the reduction of Pt ions readily occurs on the tops of the nanorods. As a result, the resultant hollow nanotubes (wall thickness $\approx$ 30 nm) displayed an external diameter that decreased in size from top to bottom (see Figure 4A). In terms of the epitaxial growth process, sparse platinum nanoflakes (upper inset, Figure 4A) grew from the nucleated islands and their sizes were larger at the top and gradually decreased to the bottom, resembling the concentration gradient of the H_2PtCl_6 solution. The thicknesses of the nanoflakes were estimated to range from 2 nm to 5 nm (a thickness of $\sim$7−18 atoms). The magnified TEM images exhibit an ordered crystal lattice (upper inset, Figure 4B) with 0.25 nm lattice fringes. Fast Fourier transform (FFT) image analysis (lower inset, Figure 4B) indicated that the nanoflakes were [111] single crystalline.

To demonstrate the increased surface-area:mass ratio and enhanced electrocatalytic activity of the hollow platinum nanotube arrays, compared to platinum nanorod arrays with the same lengths (2.0 μm), the representative cyclic voltammograms (CVs) were obtained (at 50 mV/s) from −0.2 V to 1.0 V vs Ag/AgCl in 0.1 M sulfuric acid (see Figure 5A). The oxidation of platinum starting at 0.6 V in the positive scan direction is a well-known feature of bare platinum electrochemistry. The cathodic removal of platinum oxide at 0.5 V for smooth platinum nanorods is clearly observable, which is shifted to 0.4 V for hollow platinum nanotubes. This negative shift is correlated to the roughened platinum surface, which is partly due to a stronger oxide (Pt−O and Pt−OH) formation.[6a] This observation is consistent with the results from X-ray scattering and CVs of small spherical nanoparticles.[13] The mass-normalized surface area of the hollow nanotube arrays (calculated from the reversible hydrogen charge in the so-called "hydrogen underpotential window" for the polycrystalline platinum surface, from 0.0 V to −0.2 V) was more than five times greater than that of the solid nanorod arrays. The hollow platinum nanotube arrays exhibit interesting electrocatalytic activities toward adsorbed CO electro-oxidation, as represented in Figure 5B. The adlayer of CO was formed by CO gas bubbling into the solution and was then degassed by N_2 purging. As expected, the hydrogen adsorption features from 0.0 V to −0.2 V disappeared, because of the presence of chemisorbed CO, yielding flat profiles. There is an obvious difference in the CO electro-oxidation current density on the hollow platinum nanotubes and the platinum nanorods. The anodic oxidation of CO to CO_2 on hollow platinum nanotubes is strongly promoted, evident by the lower onset potential at 0.4 V, compared at 0.5 V on platinum nanorods (see Figure 5B), as well as the anodic peak position shift to lower potential

(10) Yin, Y. D.; Rioux, R. M.; Erdonmez, C. K.; Hughes, S.; Somorjai, G. A.; Alivisatos, A. P. *Science* **2004**, *304*(5671), 711–714.
(11) Fan, H. J.; Knez, M.; Scholz, R.; Hesse, D.; Nielsch, K.; Zacharias, M.; Gosele, U. *Nano Lett*. **2007**, *7*(4), 993–997.
(12) (a) Sun, Y.; Xia, Y. *J. Am. Chem. Soc*. **2004**, *126*(12), 3892–3901. (b) Sun, Y.; Mayers, B. T.; Xia, Y. *Nano Lett*. **2002**, *2*(5), 481–485. (c) Chen, J.; McLellan, J. M.; Siekkinen, A.; Xiong, Y.; Li, Z.-Y.; Xia, Y. *J. Am. Chem. Soc*. **2006**, *128*(46), 14776–14777. (d) Robinson, R. D.; Sadtler, B.; Demchenko, D. O.; Erdonmez, C. K.; Wang, L.-W.; Alivisatos, A. P. *Science* **2007**, *317*(5836), 355–358.
(13) (a) Mukerjee, S.; McBreen, J. *J. Electroanal. Chem*. **1998**, *448*, 163. (b) Park, S.; Wasileski, S.; Weaver, M. J. *J. Phys. Chem. B* **2001**, *105*, 9719.

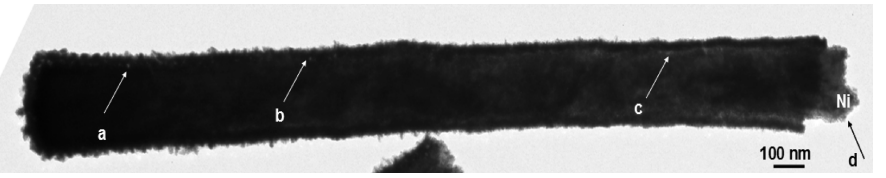

Figure 3. Intermediate state of replacement reaction, including (a, b) interfacial Kirkendall voids, (c) the separated interfacial vacancy, and (d) the nickel core.

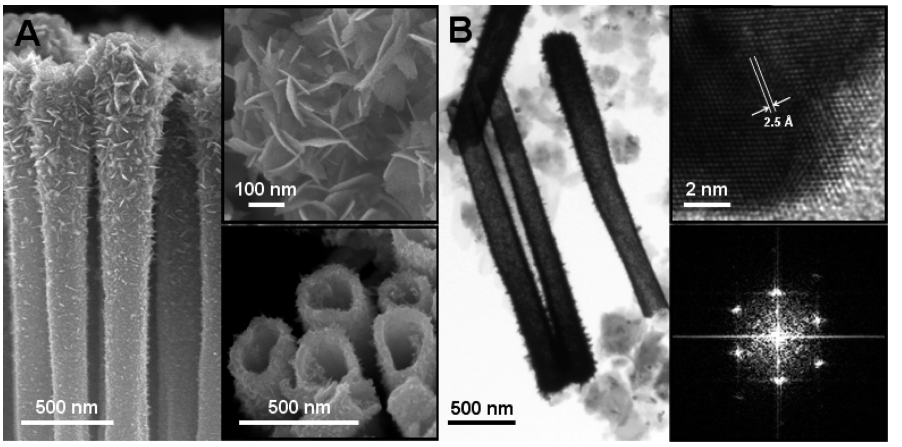

Figure 4. (A) SEM images of vertical hollow platinum nanotubes array (A) including a closeup of thin superficial nanoflakes (upper right inset) and broken hollow nanotubes (lower right inset). (B) TEM images of hollow nanotubes, with a high-resolution TEM view of a partial nanoflake (upper right inset) and its Fourier transform image (lower right inset).

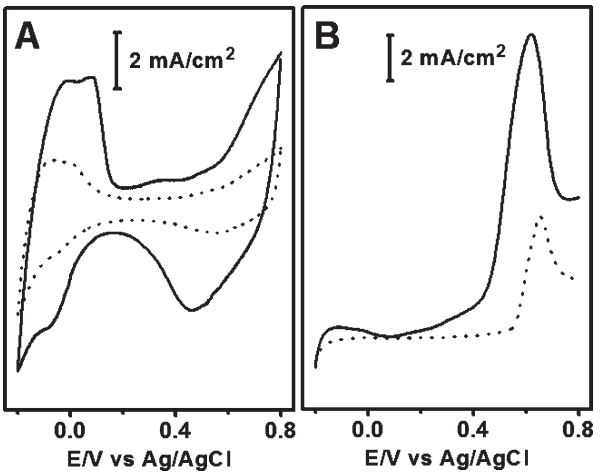

Figure 5. (A) CVs of a vertical array of platinum nanotubes (solid line) and nanorods (dashed traces). (B) Anodic scanning of electro-oxidation of irreversibly adsorbed CO molecules. All CVs were obtained in 0.1 M H_2SO_4 aqueous solution with a scan rate of 50 mV/s, vs a Ag/AgCl reference electrode.

(0.61 V for the platinum nanotube and 0.65 V for the platinum nanorod). There are two possible explanations for the observed promotion. One is the high energies on edges of nanoflakes generated on the rough platinum nanotube surfaces, and the other is the catatlytic activity promotion endowed by the presence of a trace amount of nickel within the matrix of Pt atoms. These may contribute to the lower CO oxidation potential shift, although more study is required to unveil the exact reason. The higher anodic current density originates from the effective surface area of hollow platinum nanotubes covered with thin nanoflakes being larger than that of a smooth platinum nanorod array electrode of the same length.

Conclusion

In summary, we have demonstrated that vertical hollow platinum nanotube arrays can be readily fabricated in light of synergistic pitting corrosion, the Kirkendall effect, and galvanic replacement. The product shows higher electrocatalytic activity in the case of CO oxidation. This simple synthetic mechanism could offer a promising avenue for the syntheses of a wide range of advanced hollow nanostructures. Furthermore, this example may be used as a guide in the modulation of the dimensionality of rodlike nanostructures in the radial and axial directions and allow for the expedient preparation of single-crystalline objects in an aqueous solution at room temperature.

Acknowledgment. This work was supported by the National Research Foundation of Korea (World Class University (WCU): R31-2008-000-10029-0, Nano R&D Program: 2009-0083199, 2009-0069354, and Priority Research Centers Program: NRF-20090094025).

Supporting Information Available: Figure showing the morphology of the platinum nanorods after galvanic replacement. This material is available free of charge via the Internet at http://pubs.acs.org.